This is a “preproof” accepted article for Mineralogical Magazine.
This version may be subject to change during the production process.
10.1180/mgm.2025.18

Mineralogical characteristics of *ex* and *in situ* heat treated cherts

María de Uribe Zorita[1*], Pedro Álvarez-Lloret[1], Beatriz Ramajo[2], Celia Marcos[1*]

[1] Department of Geology and Enrique Moles Institute, University of Oviedo, Oviedo 33005, Spain

[2] Scientific-Technical Services, University of Oviedo, Oviedo 33005, Spain

* Corresponding authors: cmarcos@uniovi.es (C. Marcos) and uo251780@uniovi.es (M. de Uribe Zorita, PhD student)

Abstract

Eleven chert samples from various geographical and geological locations and ages were *ex situ* heat treated, with two samples also undergoing *in situ* heat treatment. Characterization was performed using X-ray fluorescence (XRF), X-ray diffraction (XRD), and Raman spectroscopy. The results indicated that the presence of moganite in cherts is independent of whether they are quartzitic or cristobalitic/tridymitic. *Ex situ* heat treated cherts cannot be differentiated by type, as they may all contain quartz, cristobalite, and tridymite. Heat treatment induced transformations in both siliceous and non-siliceous phases, forming new crystalline phases. The observed transformations at 1000 ºC agree with literature data. XRD and Raman spectroscopy are crucial for comprehensive chert analysis, with Raman detecting lower concentrations and textural variations. A correlation exists between chert type (quartzitic or cristobalitic/tridymitic), i.e., mineralogical composition, and age, but not between elemental composition and age. The dynamics of *ex situ* and *in situ* heating of cherts lead to distinct crystalline transformations. These transformations can significantly affect the properties of the cherts. Analytical tools used to characterize the mineral phases of cherts are a fast and efficient alternative to conventional petrographic microscopy, especially in the case of heat-treated cherts.

Keywords: Chert, *ex situ* heat treatment, *in situ* heat treatment, XRD, Raman spectroscopy

1. Introduction

Cherts, dense, very hard, fine-grained sedimentary rocks, are mainly composed of microcrystalline or cryptocrystalline siliceous mineral phases, making up more than 90% of their composition; cherts often contains visible fossils of diatoms, radiolarians, and sponge spicules, varying greatly in color, from white to black. Cherts can have a uniform texture and a relatively simple mineral composition, although their formation process can be extremely complex. Chert outcrops are often found intercalated with host formations like limestone, and they typically present as bedds or nodules. Stratified cherts are primarily linked to inorganic and/or biogenically induced precipitation (Kuma et al. 2019), while nodular cherts form through complex interactions between depositional processes and diagenetic alterations (Shen et al., 2018; Dong et al., 2020; Lampropoulou et al., 2022). Cherts are common in the geological record, from the Precambrian to the Quaternary periods (Boggs, 2009; Tucker, 2001), but not abundant. Chert deposits are resilient to diagenetic changes, making them valuable records of environmental (Adachi et al., 1986; Murchey and Jones, 1992; Murray, 1994) and diagenetic (Shen et al., 2018; Tatzel et al. 2015) sedimentary processes. The source of SiO_2 is believed to be either entirely from biological origin or a result of hydrothermal activity (Maliva et al., 2005; Shen et al., 2018). From the Archean Eon to the Paleoproterozoic (4000 Ma to 1600 Ma), chert precipitated abiotically from seawater to the ocean floor (Maliva et al., 2005). During the Mesoproterozoic and Neoproterozoic eras (1600 Ma to 541 Ma), cherts formed in carbonate beds. Biogenic cherts emerged in the late Proterozoic, marked by the presence of siliceous sponge spicules (Brasier et al., 1997; Maliva et al., 2005). From the Precambrian to the Silurian (635 Ma to 443.8 Ma), cherts contained fossils replaced by silica, coinciding with the abundance and diversity of siliceous sponges (Gehling and Rigby, 1996; Kidder and Erwin, 2001). During the Cenozoic (66 Ma to present), the marine plankton shifted from radiolarians to diatoms and there was also more carbonate precipitation and less CO_2 in the atmosphere and ocean compared to earlier periods (Westacott et al., 2021). Cenozoic cherts precipitated more frequently during glacial periods (Arthur and Sageman 2003; Kidder and Erwin, 2001).

Silica, at atmospheric pressure, exists in several mineral phases. Quartz, tridymite, and cristobalite undergoe two types of changes with temperature: inversion and reconversion. Inversion involves minor structural changes without breaking bonds, occurring almost instantly and is reversible; this reaction happens during the low (α) to high (β) temperature transformation of each siliceous phase. Reconversion, on the other hand, involves breaking Si-O-Si bonds and restructuring of the Si-O tetrahedra; this reaction is also reversible, but involves significant structural reorganization and occur at an extremely slow rate. The stability ranges of these forms have been extensively studied; one of the earliest and most cited studies is by Fenner (1913), who proposed the following transformation sequence:

$$\text{Quartz} \xrightarrow{870\ ^{o}C} \text{Tridymite} \xrightarrow{1470\ ^{o}C} \text{Cristobalite} \qquad (1)$$

Pure quartz transforms into cristobalite between 1470 and 1710 ºC (Mackenzie, 1960). However, this transformation in natural silica minerals has been observed at a lower temperature range of 1100-1600 ºC (Schneider et al., 1986). Contrary to Fenner proposal, Stevens et al. (1997) argued that tridymite is not a stable phase in the pure silica system, although cristobalite may form first. The structure of tridymite depends on the origin of the samples (Silve et al., 1991). Stacking disorder of tridymite can result in line broadening, different reflection profiles, reflections shift, and changes in the intensity of X-ray diffraction (XRD) reflections (Graetsch and Flörke, 1991). Tridymite and cristobalite can coexist individually or intergrowth in the same crystal (Nukui and Flörke, 1987; Thompson and Wennemer, 1979). Several authors (Chaklader, 1963; Chaklader and Roberts, 1961) suggested that quartz passes through an amorphous transition phase before transforming into cristobalite. Kuellmer and Poe (1964) found no pronounced amorphous phase below 1550 °C and showed that the transformation was through highly fragmented quartz with high temperature dislocation content. Chaklader (1961) and Stoch et al. (1985) found that impurities such as Al^{3+} catalyze the transformation of quartz and the formation of cristobalite considerably.

On the other hand, Shoval et al. (1989) demonstrated by XRD that heating chert to 1000 °C for one hour formed a small amount of cristobalite, and at higher temperatures or longer heating times more of the cristobalite phase was formed. According to Shoval et al. (1997), cherts are rocks rich in crystalline defects, which serve as nucleation sites, allowing early quartz-cristobalite transformation.

Moganite is a polymorph of silica and a very common component of microcrystalline silica rocks (Flörke et al., 1984). Heaney (1995), based on the frequency of occurrence of moganite and its associations, established that moganite disappears with age as it is very rare or absent in pre-Cretaceous rocks. Parthasarathy et al. (2001) demonstrated that moganite is also a common mineral in hydrothermal environments. Several authors (Heaney and Post, 2001; Heaney et al., 2007) indicated a phase transition of monoclinic-to-orthorhombic moganite between 296 and 316 °C, while between 900 and 1000 °C it transformed to cristobalite (Flörke et al., 1984; Miehe and Graetsche, 1992).

In this study, the thermal behavior of several cherts of different ages and compositions has been investigated in order to establish possible differences between them. From a geological point of view, the aim is to establish possible differences between the origin and age of the cherts and their response to heat treatment.

2. Experimental

2.1. Materials and treatments

Eleven chert samples from different provenences and geological periods were selected for *ex situ* heat treatment:

- NMNH-117787-35 (46º1’18.28’’N 111º16’49.03’’W) and NMNH-117787-34 (46º1’18.28’’N 111º16’49.03’’W) chert from Montana (USA) (Mississippian period) appears in two formations: (i) Lodgepole Formation, which shows a significant chert content, especially in its lower sections where chert-rich organic black shales predominate. (ii) Three Forks Formation, where shale and dolomite units are interbedded with chert-rich levels, particularly in the deeper, more stable areas of the sedimentary basin during the Early Mississippian period. The chert deposition was in relatively deep and anoxic marine settings. The distribution of chert in these formations is variable and is influenced by the palaeogeography and sedimentary dynamics of the area during the Mississippian. (https://scholarworks.montana.edu/items/06381099-45c3-4763-b0ed-6f4c724476d6?show=full; https://gis-data-hub-mbmg.hub.arcgis.com/apps/53bf38cf17fd45dbbcf93b6cafaa3365/explore; https://scholarworks.montana.edu/handle/1/8851).

- NMNH-117737-58 from the area between Lake Valencia (Lago Tacarigua) (10º10’58.8’’N 67º43’58.8’’W) and Guaricó (Guaricó) (8º40’0.12’’N 66º34’59.88’’W) in the Llano Central of Venezuela. In the surrounding areas of the lake, several rock formations (Tinaco Complex and Fillita de Tucutunemo), including igneous and metamorphic rocks, can be found. Both units are cut by faults (Manrique and La Victoria) which, in turn, affect the Jurassic and Cretaceous. These rocks are testimony to the complex geological history of the region, with a predominance of thrust faults. The sub-basin is associated with the Guaricó fault system, which overlies Cretaceous and Tertiary rocks, creating a complex tectonic framework. Guaricó Formation: The soils of this region belong to the Guaricó Formation, which consists mainly of thin layers of sandstones and siltstones, alternating with layers of shales and mudstones (USGS, 2006).

- 7219 (44º55’13.35’’N 0º12’8.72’’W) from Libourne which is located in the Cretaceous sedimentary deposits, at the confluence of the Isle and Dordogne rivers (France). During the Cretaceous, the region was covered by shallow seas. This environment favoured the accumulation of marine sediments, the formation of characteristic sedimentary rocks and the preservation of marine fossils. This Basin (65.000 km²) has been gradually filled with sediments over the last 250 million years. It includes alternating layers of sand, silt, carbonates and clays.

- 16681 (41º19’16.61’’N 0º51’25.40’’E) from the Ulldemolins Complex Formation (Tarragona, Spain), which is dated to the Rupelian-Chattian (Oligocene). This formation was deposited in continental lacustrine environments, not in shallow seas (Roqué and Terradas, 2016). The Ulldemolins chert has the following characteristics: It occurs in the form of nodules within limestones. It contains fossils of freshwater organisms such as gastropods, ostracods, carophyceans and fish. It was formed in a marginal sedimentary basin disconnected from the Ebro basin, on the Pyrenean overriding bed. The silica probably came from the dissolution of the remains of siliceous freshwater organisms or from silica-rich groundwater inputs. The diagenetic processes of dissolution and reprecipitation of the silica led to the formation of the nodules of chert within the lacustrine limestones IGME (1973).

- 18185 from Sant Pere de Riudebitlles, located in the Alt Penedès region of Barcelona (Spain) (41º27’09’’N 1º42’17’’E), has an interesting and varied geology. The region is characterised by sedimentary formations that originated mainly during the Cretaceous. These formations include limestones, marls and chert, which were formed in shallow marine environments. The terrain of Sant Pere de Riudebitlles is influenced by the fluvial activity of the river Bitlles, which has contributed to the formation of alluvial terraces and fluvial deposits. These deposits are rich in sedimentary materials that have been transported and deposited by the river over time. In addition, the region shows evidence of the Hercynian orogeny, a tectonic event that affected much of Europe during the Palaeozoic. This orogeny left a base of metamorphic and magmatic rocks on which the more recent sedimentary layers were deposited (IGME (1972).

- 26407 from upper Cretaceous (Cenomanian to Turonian) chert-bearing marlstones in the region of Lorca, Murcia (Spain), are found in several geological formations. One of the prominent areas is the Sierra de la Tercia, north of Lorca (37º48’0’’N 1º42’0’’W) (IGME,1972).

- La Marañosa (B and BE) (40º16’35.04’’N 3º34’4.08’’W) from La Marañosa located in the municipality of San Martín de la Vega, near Getafe (Madríd, Spain), belongs to the Miocene (Upper Vindobonian) (IGME,1973).

- Cerro Almodóvar (B and NB) (40º23’9.96’’N 3º35’56.04’’W) from Cerro Almodóvar located in the district of Vicálvaro in Madrid (Spain), it is a witness hill that stands out in the surrounding plain due to its resistance to erosion. This hill was formed during the Miocene (Aragonian) through sedimentary and chemical processes. During the Miocene, the regions of San Martín de la Vega and Cerro Almodóvar were influenced by sedimentary environments that favoured the formation of chert and other minerals such as sepiolite. Chert was formed from the accumulation of the remains of silica-rich marine organisms, such as diatoms and sponges, which were compacted and transformed into nodules through diagenesis processes (IGME (1986). Table 1 summarises the provenance, geological period and geological context of the cherts investigated.

Table 1. Summary of the provenance, geological period and geological context of the cherts investigated.

Sample	Provenance	Geological Period	Geological Context
NMNH-117787-35	Montana (USA)	Mississippian (Carboniferous)	Lodgepole and Three Forks Formations, deep marine, anoxic conditions
NMNH-117787-34	Montana (USA)	Mississippian (Carboniferous)	Lodgepole and Three Forks Formations, deep marine, anoxic conditions
NMNH-117737-58	Northern Guarico-Lake Valencia Area (Venezuela)	Cretaceous	Guaricó Formation, sandstones, siltstones, shales, and mudstones, complex tectonic setting
7219	Libourne (France)	Cretaceous	Cretaceous shallow marine sedimentary basin, alternating sands, silts, carbonates, and clays
16681	Ulldemolins, Tarragona (Spain)	Oligocene (Rupelian-Chattian)	Lacustrine limestones, freshwater fossils, diagenetic silica reprecipitation
18185	Sant Pere de Riudebitlles, Barcelona (Spain)	Cretaceous	Cretaceous shallow marine deposits, Hercynian orogeny influence
26407	Lorca, Murcia (Spain)	Upper Cretaceous (Cenomanian to Turonian)	Chert-bearing marlstones in Sierra de la Tercia
La Marañosa B	Getafe, Madrid (Spain)	Miocene (Upper Vindobonian)	Miocene sedimentary deposits, silica from diatoms and sponges
La Marañosa BE	Getafe, Madrid (Spain)	Miocene (Upper Vindobonian)	Miocene sedimentary deposits, silica from diatoms and sponges
Cerro Almodóvar B	Vicálvaro, Madrid (Spain)	Miocene (Aragonian)	Miocene witness hill, erosion-resistant deposits, sepiolite and silica-rich sedimentation
Cerro Almodóvar NB	Vicálvaro, Madrid (Spain)	Miocene (Aragonian)	Miocene witness hill, erosion-resistant deposits, sepiolite and silica-rich sedimentation

The *ex situ* heat treatment was carried out in a Carbolite CWF 12/23 furnace (Área de Cristalografía y Mineralogía, Universidad de Oviedo) with a heating ramp at a controlled rate of 5 ºC/min until reaching 1000 ºC, this temperature was maintained for 48 hours, and then cooling was carried out at the same rate. Temperature calibration is tested periodically with certified equipment by Carbolite factory qualified personal. For *in situ* heating of the samples, Cerro Almodóvar B and La Marañosa BE, the Anton Paar HTK1200N chamber was used with the diffractometer specified below. Heating ramps up to 1000 ºC were performed at a controlled rate of 5ºC/min.

3. Characterization

The characterization of the samples was carried out using several techniques (X-ray fluorescence, X-ray diffraction, and Raman spectroscopy) to determine the chemical and mineral composition and its variations and crystalline structure. All of the characterizations were performed at room temperature except the *in situ* heat treatment.

The composition of the elements expressed in oxides (%) of the chert samples - NMNH-117787-35, NMNH-117787-34, NMNH-117737-58, 7219, 18185, 26407 - was taken from Uribe-Zorita et al. (2023). The chemical composition of the other cherts has been obtained by X-ray fluorescence with a Shimadzu EDX-720 equipment following the same methodology.

The diffractogram patterns of the starting and *ex situ* heat treated samples were recorded with the diffractometer PANalytical X´Pert Pro MPD. The diffractogram patterns of the *in situ* heat treated samples were acquired with the PANalytical X'Pert Pro MPD diffractometer coupled to a controlled heating chamber (Anton Paar HTK1200N). PANalytical X'Pert MPD Pro was configured in Bragg-Bretano with fixed, primary divergence and antiscatter slits of 1º and 2º aperture respectevely. Diffraction patterns were recorded at 40 mA and 45 kV (Cu K_α radiation; λ = 1.5418 Å) on scanning mode over 5 to 86 º(2 theta) at angular velocity of 0.22 º/s by a solid state PIXcell detector. Previously, X-ray radiation was monochromatized by means a large Ni filter. Early on, Anton Paar HTK 1200N chamber were calibrated using a periclase (MgO) sample, analyzing its linear thermal expansion coefficient from room temperature to 1000ºC. Diffractogram recording was performed every 100 ºC, at stabilized temperatures (300 ºC, 700 ºC and 1000 ºC the stabilization time was

extended by 50 hours) by continuous scanning at 0.08 º/s over the angular range between 15º and 85º from 2θ. he samples, 0.5 g each, were previously ground in an agate mortar to obtain the diffractogram patterns with the powder method in the starting and *ex* and *in situ* heat treated samples. The software used to identify the mineral phases was X'Pert HighScore Plus 2.2d (2.24) 2008.

Raman spectra were obtained using a JASCO NRS-5100 spectrometer (Jasco Inc. MD, Easton, USA) equipped with a charge-coupled device detector (Andor DU 420) and coupled to an Olympus optical microscope. The Raman spectra were excited with a diode laser (λ = 785 nm) kept at 500 mW. Spectra were acquired between 100 and 800 cm^{-1} with a resolution of 1 cm^{-1}, exposure time 10 s with 10 accumulations. Spectra smoothing was performed using SYSTAT version 13 (Systat Software, Inc., San Jose CA, USA).

4. Results

4.1 X-ray fluorescence

The elemental composition of the elements expressed in oxides (wt. %) and their corresponding mass loss by ignition (L.O.I.) is in Table S1 (has been deposited with the Principal Editors of Mineralogical Magazine and is available as Supplementary material (see below)). The standard deviation (SD) was less than 0.3 for SiO_2, less than 0.5 for Al_2O_3, less than 0.1 for MgO, and less than 0.005 for the other analyzed oxides. In relation to silica content, the analyzed cherts can be differentiated into those with > 99% (7219 and Cerro Almodóvar B), those with 90 - 95% (NMNH-117787-35, NMNH-117787-34, 26407 and La Marañosa B), and those with 80 - 90% (16681, 18185, Cerro Almodóvar NB and La Marañosa BE); NMNH-117737-58 stands out with 67.87%. The Al-Fe-Mn diagram for the investigated cherts (Fig. 1a) and the representation of SiO_2 against total iron as Fe_2O_3 (Fig. 1b) both indicate that these cherts are exclusively composed of biogenic silica. Notably, they fall below the pelagic clay line, reinforcing their unique composition. An exception is the formation of sample 26407, which may have resulted from the mixing of basaltic materials and silica (Adachi 1986, Yamamoto 1987). The unusual composition exhibited by chert NMNH-117787-58, low silica content and high alumina content, is clearly reflected by its position in Fig. 1b.

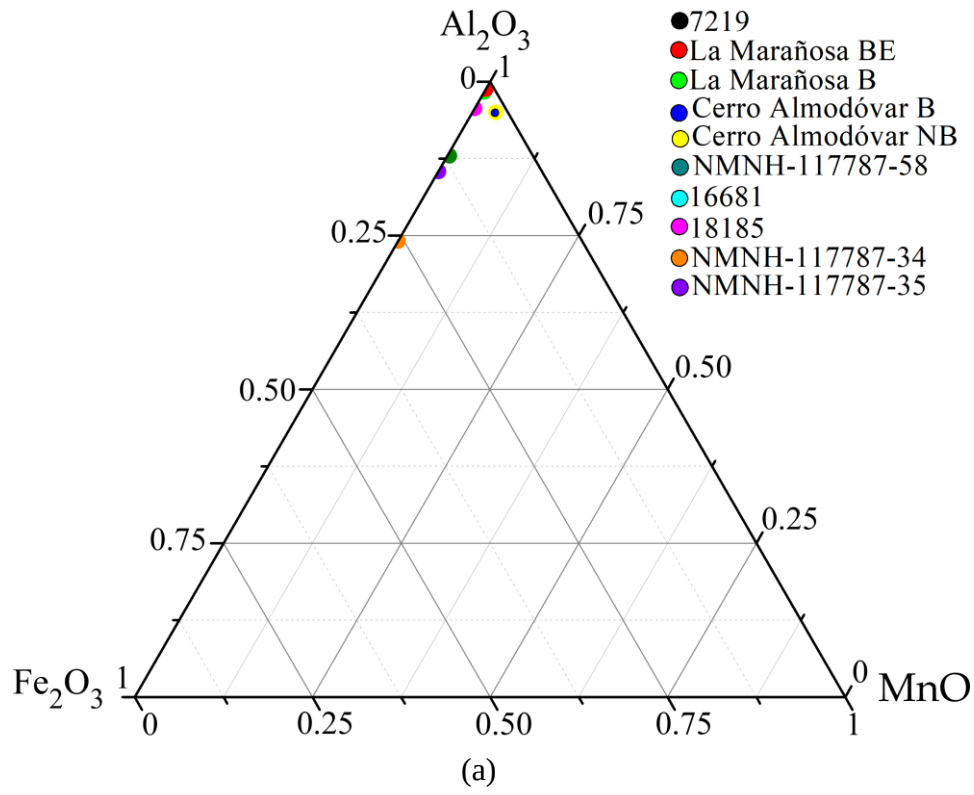

(a)

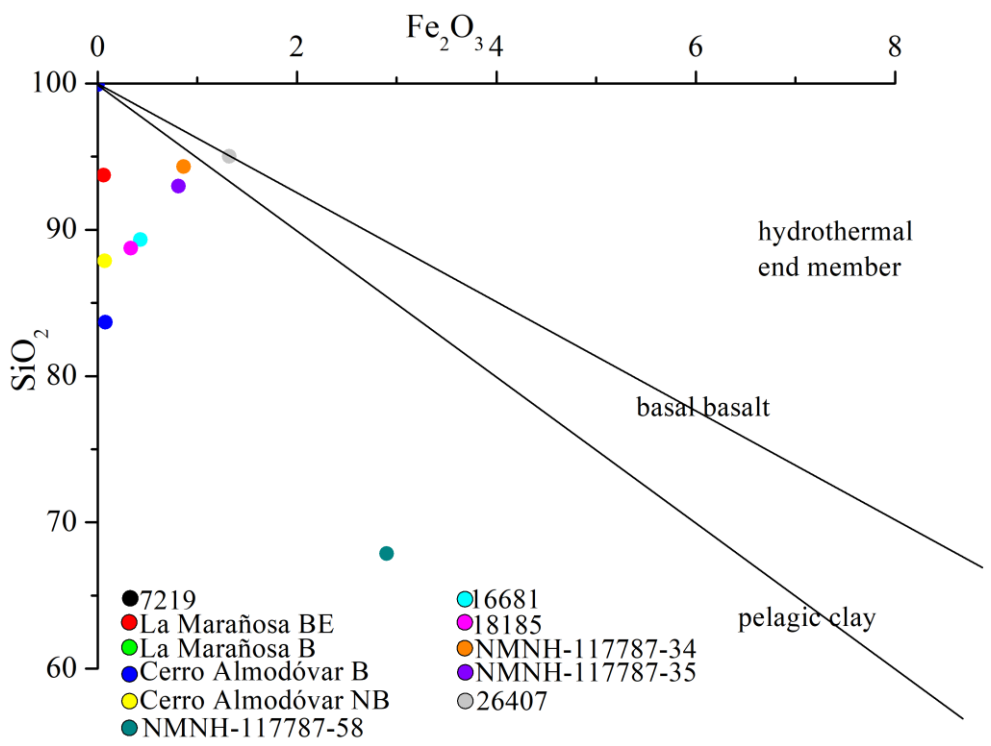

(b)

Fig. 1. (a) Al_2O_3- Fe_2O_3-MnO (wt. %) diagram showing the composition of the investigated cherts; (b) plot of SiO_2 against total iron as Fe_2O_3. The composition of pelagic clay is from Turekian and Wedepohl (1961) (the composition of basalt and hydrothermal end member was taken from Adachi et al. (1985)).

4.2 X-ray diffraction

From the XRD results of the unheated cherts, two types can be differentiated on the basis of the main phase(s) of which they are composed, quartz and/or cristobalite and/or tridymite. The quartzitic cherts (Fig. 2a) consist primarily of quartz. In contrast, the

tridymitic/cristobalitic cherts (Fig. 2b) are composed of varying proportions of quartz, cristobalite, and/or tridymite. Other phases may be present in very small proportions (moganite, calcite, dolomite, phyllosilicates, etc.) (Table S2) (Table S2 has been deposited with the Principal Editors of Mineralogical Magazine and is available as Supplementary material (see below)).

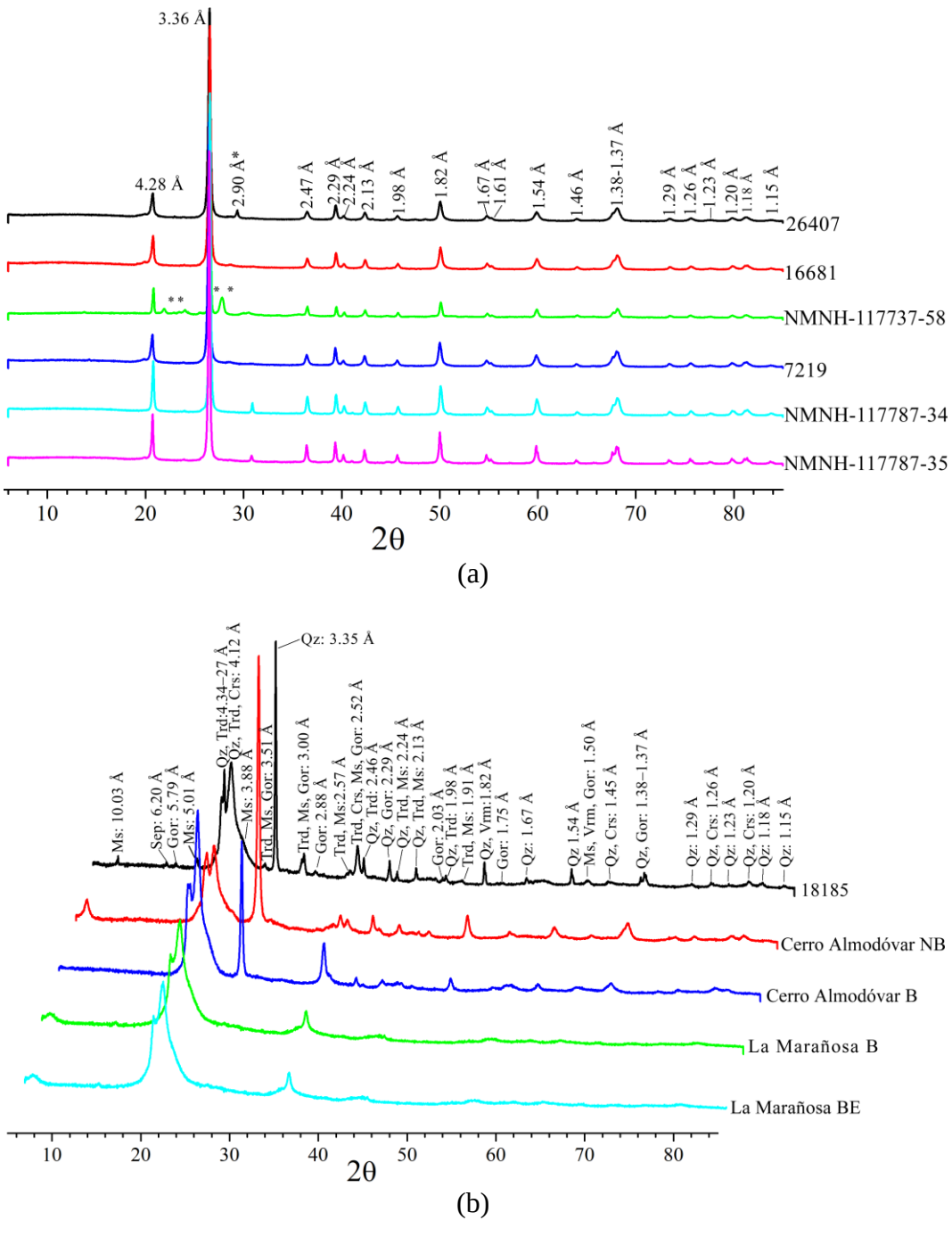

Fig. 2. XRD patterns: (a) quartzitic cherts in which the majority of the reflections correspond to quartz (Qz) and moganite (Mog), except those marked with * which correspond to dolomite (Dol) and ** which belong to albite (Ab); (b) tridymitic/cristobalitic cherts showing the reflections corresponding to the phases quartz, tridymite (Trd), cristobalite (Crs), gorceixite (Gor), sepiolite (Sep), phyllosilicates (muscovite: Ms). Mineral abbreviations taken from Whitney and Evans (2010).

XRD results of the *ex situ* heat treated cherts are presented in Fig. 3.

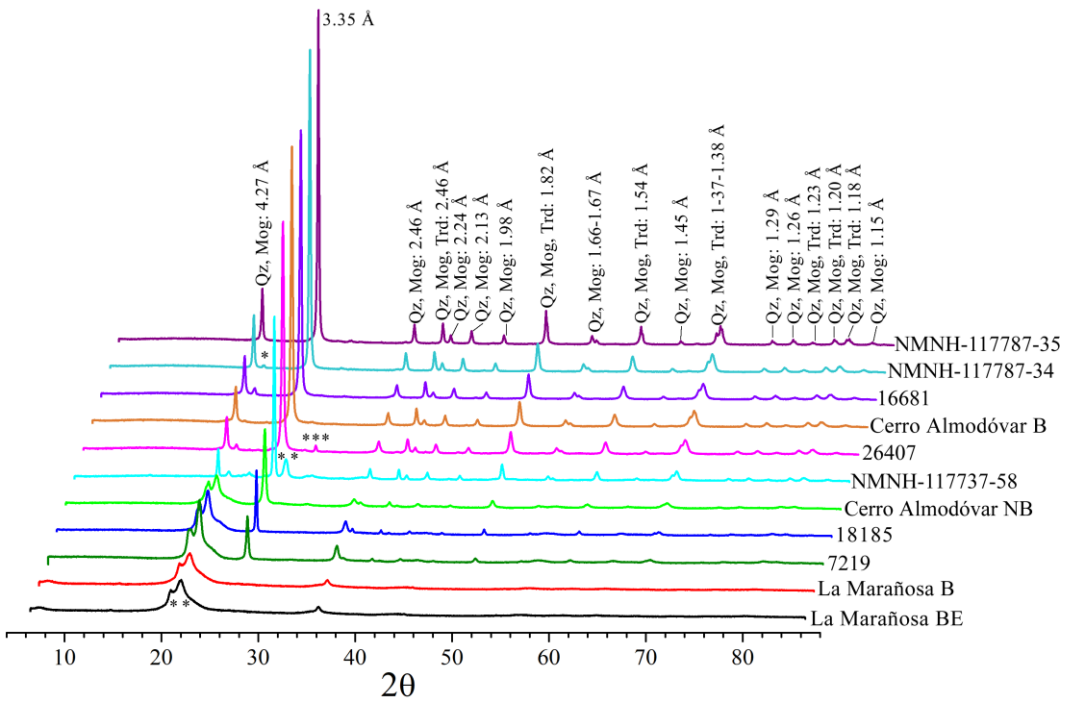

Fig. 3. X-ray diffraction patterns of *ex situ* heat treated cherts showing reflections corresponding to the phases that compose the cherts: quartz (Qz), tridymite (Trd), cristobalite (Crs), moganite (Mog) and cristobalite-tridymite (*), quartz-tridymite-cristobalite (**), tridymite and wollastonite (Wo) (***). Mineral abbreviations taken from Whitney and Evans (2010).

With heat treatment the analyzed cherts cannot be differentiated into quartzitic and tridymitic/cristobalitic because all of them may be composed of quartz, cristobalite and tridymite, in addition to other phases present in a very small proportions, such as moganite (Table S3) (Table S3 has been deposited with the Principal Editors of Mineralogical Magazine and is available as Supplementary material (see below)).

XRD patterns of *in situ* heat treated samples of Cerro Almodóvar B and La Marañosa BE are shown in Fig. 4a,b, respectively.

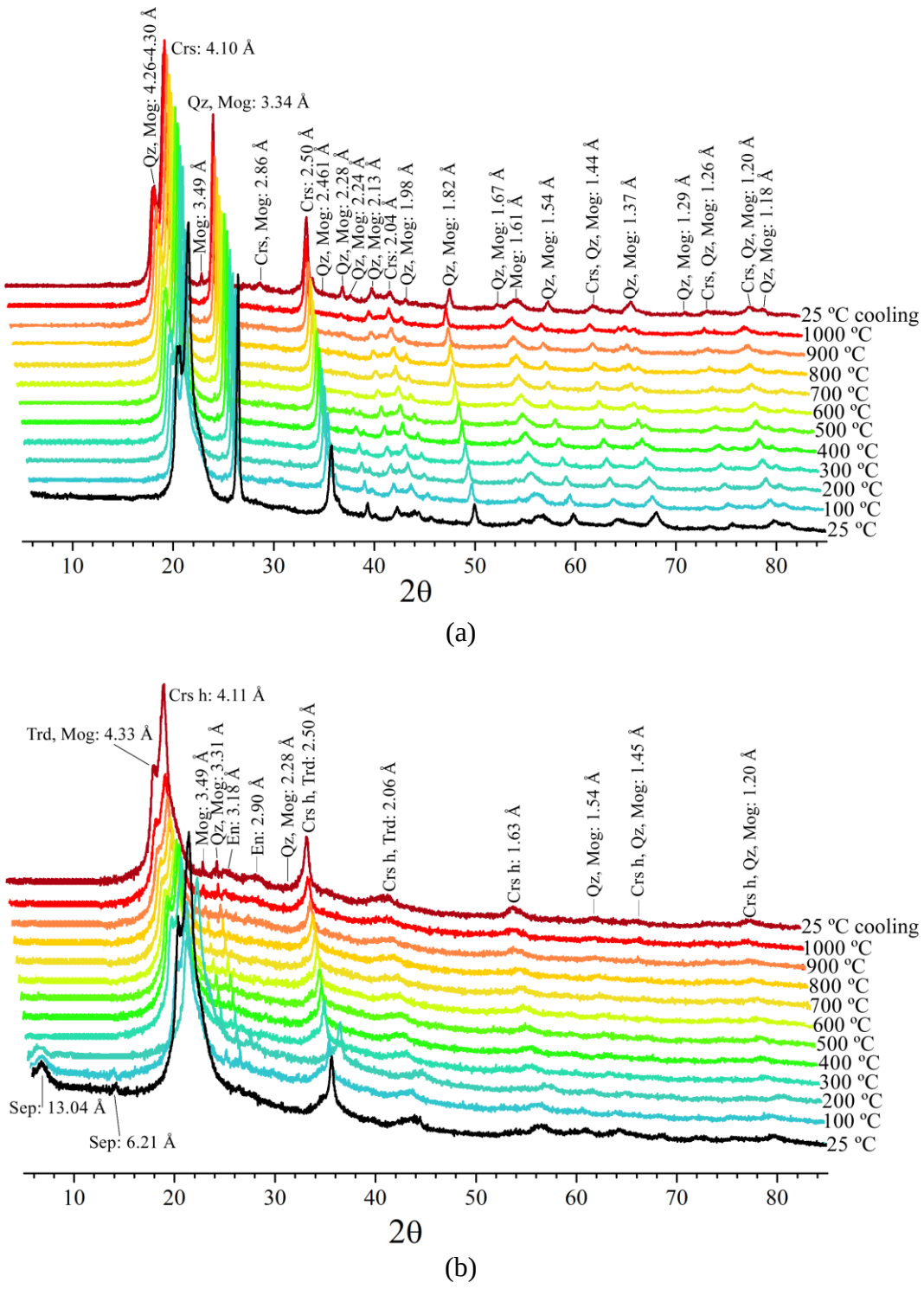

Fig. 4. XRD patterns of the *in situ* heated Cerro Almodóvar B sample (a) and La Marañosa BE sample (b). Mineral abbreviations - quartz (Qz), tridymite (Trd), cristobalite (Crs), moganite (Mog), sepiolite (Sep), enstatite (En)- were taken from Whitney and Evans (2010).

The intensity of reflections from both quartz (JCPDs 5-490) and tridymite (JCPDs 18-1169) of the *in situ* heat treated Cerro Almodóvar B sample increase from 25 ºC to 100 ºC; at 200 ºC tridymite transformed to cristobalite (JCPDs 1-424); up to 400 ºC the intensity of these reflections increased; at 500 ºC cristobalite transformed to cristobalite high (JCPDs 27-605) and low quartz transformed to quartz high (JCPDs 11-252); at 600 ºC the reflections intensity decreased; at 700 ºC the intensity of reflections increased considerably and at 800 ºC decreased considerably, increased significantly again to 900 °C; on cooling to 25 ºC the reflections decreased slightly and cristobalite high and quartz high transformed to cristobalite low and quartz low. Moganite (JCPDs 38-360 and/or AMCSD-2737, AMCSD-2738, AMCSD-6460) was always present (Fig. 4a). The slope shown between 20º - 30º of 2θ indicates crystallinity loss of the sample. The gradual change in the 2θ value of the (101) quartz reflection and 2θ value of the (111) cristobalite reflection caused by heating the chert up to 1000 ºC is shown in Table 2. The variation of the FWHM (Full Width at Half Maximum) values of the (101) quartz reflection and the principal (111) cristobalite reflection with temperature is also shown in Table 2. The FWHM of the (101) quartz reflection varied with temperature but there is no clear trend. The (111) cristobalite reflection slightly decreased with increasing temperature but also increased after cooling. The FWHM values of the (111) cristobalite reflection significantly decreased with increasing temperature, reaching its lowest value around 400 °C, and then then varied without a clear trend.

Table 2. Values of 2θ and FWHM of values for quartz reflection (101) and cristobalite reflection (111) for Cerro Almodóvar B sample.

	Quartz		Cristobalite	
T (ºC)	2θ (101) reflection	FWHM (º2θ)	2θ (111) reflection	FWHM (º2θ)
	26.60	0.15	21.65	0.38
100	26.57	0.17	21.58	0.33
200	26.53	0.13	21.54	0.09
300	26.45	0.17	21.50	0.08
400	26.42	0.18	21.50	0.06
500	26.38	0.14	21.54	0.13
600	26.34	0.13	21.54	0.18
700	26.34	0.18	21.54	0.06
800	26.38	0.14	21.58	0.13
900	26.34	0.19	21.58	0.08
1000	26.38	0.09	21.58	0.06
after cooling	26.65	0.14	21.73	0.09

The diffractogram pattern of the *in situ* heat treated La Marañosa BE between 100 and 1000 ºC shows that cristobalite (JCPDs 27-605) is the major phase and quartz is minor (JCPDs 5-490); tridymite (JCPDs 16-152) and moganite (JCPDs 38-360) also may be present.

The intensity of cristobalite reflections decreased from 25 ºC to 100 ºC, increased between 500 and 600 ºC, and then decreased slightly again up to 1000 ºC; after cooling, at 25 ºC, it increased slightly. The slope shown between 20º and 30º from 2θ indicates very low crystallinity of the sample. The 2θ and FWHM values of the quartz reflection (101) and cristobalite reflection (111) for La Marañosa BE sample are presented in Table 3. The quartz reflection (101) stabilizing around 26.80-26.88 at higher temperatures suggests that the quartz structure becames more stable and consistent as the temperature increases. The FWHM of the quartz reflection (101) showed some variation, with a notable dip at 800°C. The (111) cristobalite reflection remained fairly constant around 21.58 across all temperatures, with a slight increase after cooling. The FWHM of (111) cristobalite reflection showed significant variation, with higher values at lower temperatures and a decrease around 200-300°C, followed by fluctuations at higher temperatures.

Table 3. Values of 2θ and FWHM of values for quartz reflection (101) and cristobalite reflection (111) for La Marañosa BE sample.

	Quartz		Cristobalite	
T (ºC)	2θ (101) reflection	FWHM (º2θ)	2θ (002) reflection	FWHM (º2θ)
25	0	0	21.61	0.57
100	26.88	0.10	21.58	0.21
200	26.88	0.09	21.58	0.18
300	26.88	0.08	21.58	0.36
400	26.88	0.10	21.58	0.56
500	26.84	0.10	21.58	0.46
600	26.88	0.15	21.58	0.46
700	26.80	0.10	21.58	0.56
800	26.80	0.05	21.58	0.41
900	26.80	0.10	21.58	0.41
1000	26.80	0.10	21.58	0.51
after cooling	26.88	0.10	21.60	0.51

The diffractogram patterns of Cerro Almodóvar B and La Marañosa BE were plotted by projection with level curves and false color with Xpowder software (Martin, 2004) to visualize phase transformations, using refinement methods (based on stacking the different temperature conditions considered) through the internal calculations of the parameter-shift method (Bhuiya and Stanley, 1963). This 2D representation calculated by quadratic interpolation methods and showing different intensity scales, requires all diffractograms have been recorded under the same experimental conditions. In the 2D representation with false color of the *in situ* thermal difractogram pattern of Cerro Almodóvar B sample (Fig. 5) transformations between 100-200 ºC, 500-600 ºC and 800-900 ºC can be observed.

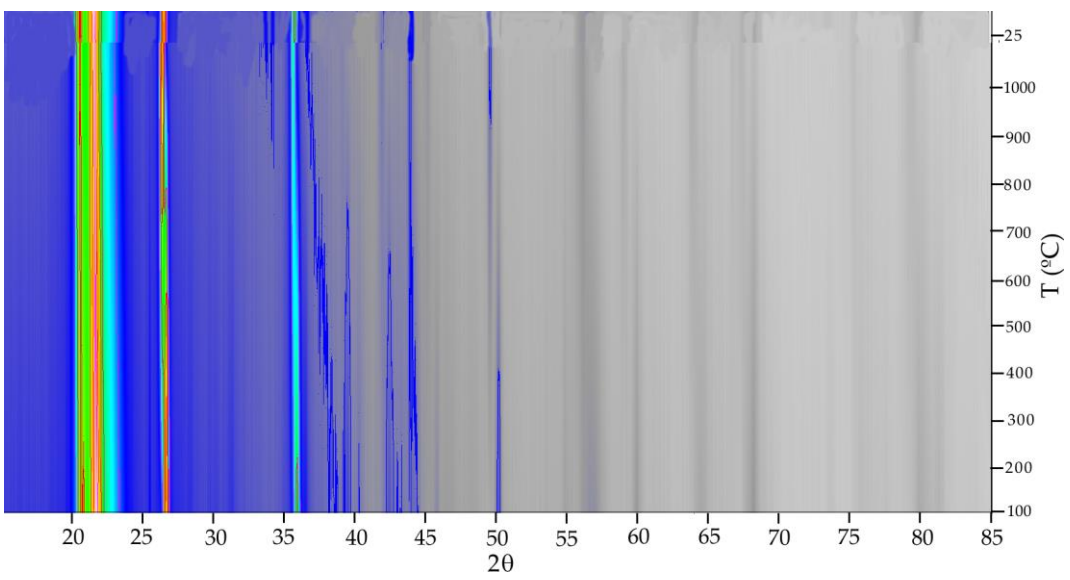

Fig. 5. Two-dimensional representation with false color of the *in situ* thermal difractograms patterns of Cerro Almodóvar B sample.

In the 2D representation with false color of the *in situ* thermal difractogram pattern of La Marañosa BE sample (Fig. 6) it can be observed transformations between 500-600 ºC and at 900 ºC approximately. At 100 ºC, tridymite transforms into cristobalite, reducing the intensity of its main reflection, while quartz begins to appear. In Fig. S1 (Fig. S1 has been deposited with the Principal Editors of Mineralogical Magazine and is available as Supplementary material (see below)) can be observed the asymmetry due to the differences in the reflections before heating to 1000 ºC *in situ* and the equivalent reflections at 25 ºC during cooling.

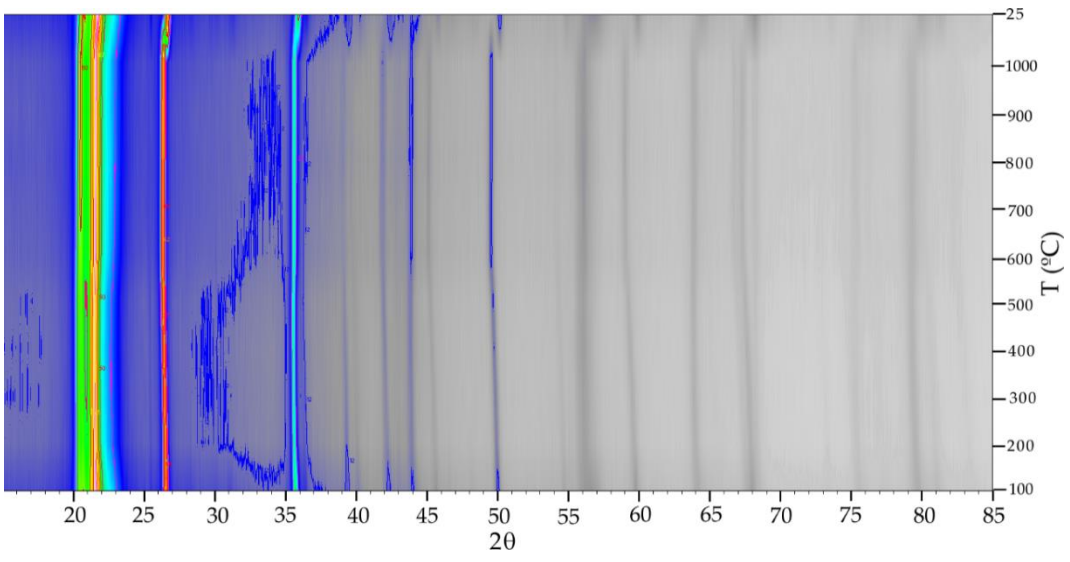

Fig. 6. Two-dimensional representation with false color of the *in situ* thermal difractograms patterns of La Marañosa BE sample.

4.3 Raman spectroscopy

The Raman spectrum section selected between 420 and 520 cm^{-1}, of the starting and *ex situ* heat treated samples is shown in Fig. 7a for the quarzitic cherts and Fig. 7b for the tridymitic/cristobalitic cherts. The more intense band at 462 cm^{-1} is associated with the presence of quartz (Kingama and Hemley, 1994; Sitarz et al., 2014), and the band visible around 501 cm^{-1} is associated with the presence of four-member rings in the moganite structure and it is the analytical band (Sitarz et al., 2014; Götze et al., 1998). The intensity of the Raman spectra of the samples heated at 1000 °C is significantly lower than that of the starting samples.

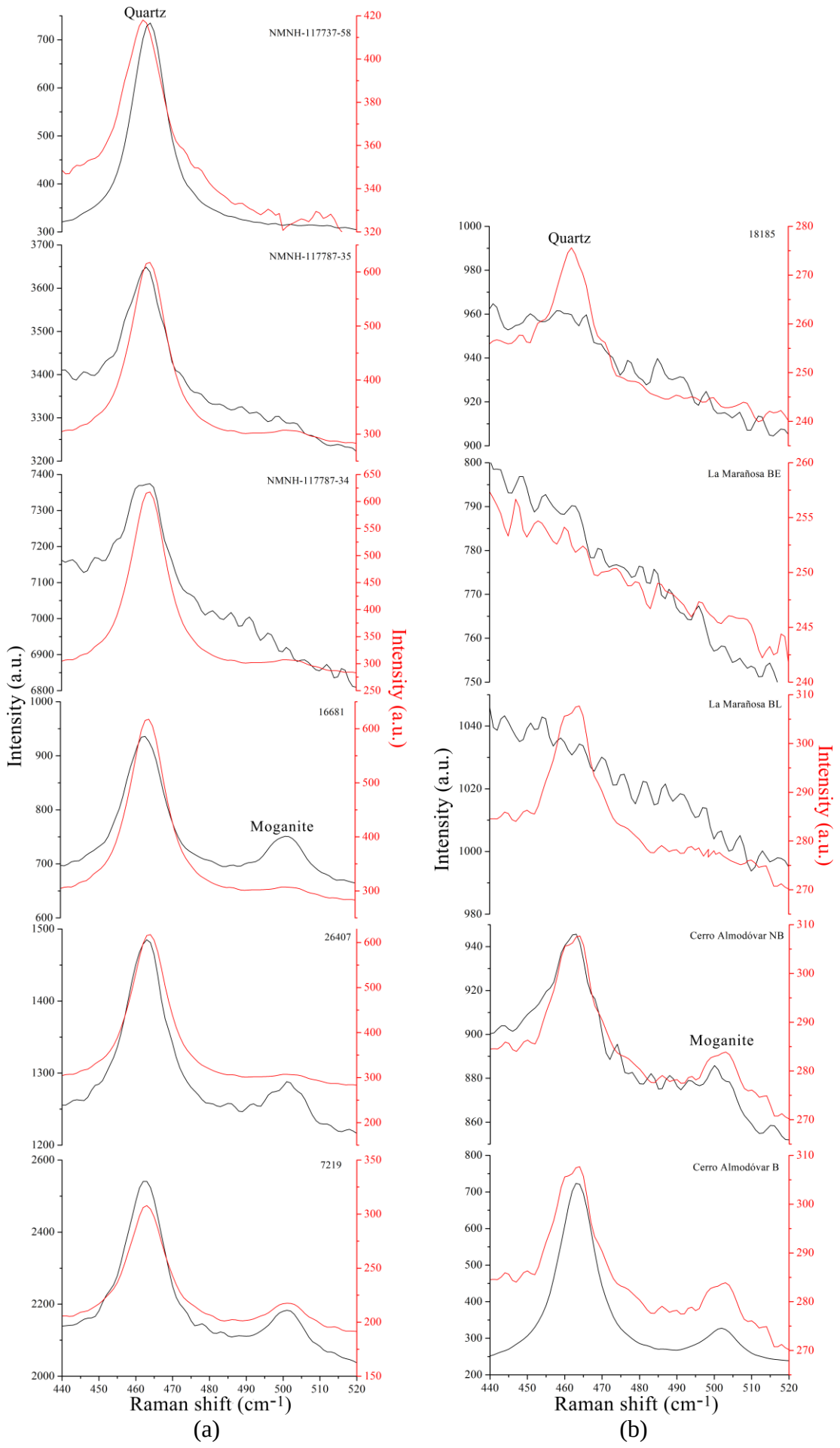

Fig. 7. Raman spectra of starting (black) and *ex situ* heat-treated (red) samples between 420 and 520 cm^{-1} showing the band corresponding to moganite (~ 500 cm^{-1}) and quartz (~ 463 cm^{-1}), (a) quartzitic cherts and (b) tridymitic/cristobalitic cherts.

5. Discussion

The presence of moganite in the cherts is independent of the type of chert (quartzitic or cristobalitic/tridymitic) but in the cherts that do not contain quartz, moganite was not detected by XRD or Raman spectroscopy. In addition, the detection of moganite by Raman spectroscopy coincides with its identification by X-ray diffraction in the starting cherts investigated. The decrease in the Raman vibrational

mode characteristic of moganite on *ex situ* heating at 1000 °C of the cherts containing it could be due to the symmetry change that occurs at 300 °C. With Raman spectroscopy was also possible to observe variations in the moganite content within the same chert sample, because this phase presents textural variations, corroborating observations made previously by Rodgers and Cressey (2001) on other types of chert. Furthermore, Raman spectroscopy is a technique with sub-micron spatial resolution capable of detecting a phase such as moganite with a concentration undetectable by ordinary XRD. This investigation corroborates that XRD and Raman spectroscopy techniques are essential and complementary in the detection and quantification of moganite (Rodgers and Cressey, 2001), a crucial phase in determining the mineralogical maturity of a chert. Also, with the XRD technique it is not necessary to use a position-sensitive detector system such as the one cited by Rodgers and Cressey (2001), as current instruments are significantly more sensitive than those used in the past.

The Miocene cherts are predominantly cristobalitic/tridymitic. The Cretaceous, Paleógeno, and Carboniferous cherts are quartzitic. A correlation is observed between chert type (quartzitic and cristobalitic/tridymitic) and age, indicating a relationship between mineralogical composition and age. However, no correlation is found between elemental composition and age.

From the data provided by the techniques used in the characterization of the investigated cherts it has been possible to describe their thermal behavior according to the process described in this study. The *ex situ* heat treated cherts, unlike the starting cherts, cannot be differentiated in quartzitic and cristobalitic/tridymitic cherts because all of them may be composed by quartz, cristobalite and tridymite. In the *ex situ* heat treated quartzitic cherts, the most important feature observed was the coexistence of low quartz and moganite with tridymite and/or high cristobalite formed by quartz transformation. On the other hand, in the *ex situ* heat treated cristobalitic/tridymitic cherts, the same siliceous phases present in these unheated cherts were maintained but some cristobalite transformed to high cristobalite. Tridymite would have formed before cristobalite (Fenner 1913), although according to Stevens et al. (1997) it would not be a stable phase and cristobalite would have formed earlier.

In summary, *ex situ* heating of quartzitic cherts would have produced the transformation of some quartz into tridymite and high cristobalite and also the transformation of some moganite with monoclinic symmetry into moganite with orthorhombic symmetry. In the case of the cristobalitic/tridymitic cherts some cristobalite would have been transformed into high cristobalite.

Additionally, both non-siliceous and silicate phases, including phyllosilicates, transformed into vitreous phases upon *ex situ* heating, some of which crystallized into new crystalline phases. The formation of wollastonite ($CaSiO_3$) in sample 26407 likely occurred at the expense of the calcite ($CaCO_3$) present in the starting sample due to decarbonation processes. The presence of anortite ($Ca(Al_2Si_2O_8)$) in the NMNH-117737-58 can be explained by the disappearance of epidote ($Ca_2(Al,Fe)_3(SiO_4)_3(OH)$) and microcline ($K(AlSi_3O_8)$) after heating the starting sample as albite ($Na(AlSi_3O_8)$) and anorthite are part of the complete solid solution of plagioclase feldspars. Diopside ($CaMg(SiO_3)_2$) likely formed in the NMNH-117787-35 at the expense of dolomite ($CaMg(CO_3)_2$) in the starting sample. Probably, sepiolite ($Mg_4Si_6O_{15}\ (OH)_2\cdot 6H_2O$) transformed into a vitreous phase during the *ex situ* heating of Cerro Almodóvar NB and La Marañosa BE samples. In the *in situ* heating of La Marañosa BE sample, transformation of sepiolite to enstatite was observed at 1000 ºC prevailing on cooling down to 25 ºC. Sepiolite loses water up to 300 ºC, rehydrates and restores its structure at 500 ºC, and transforms into protoenstatite and enstatite at 800 ºC, with enstatite prevailing up to 1000 ºC (Preisinger, 1959; Müller and Kolterman, 1965; Fernández Álvarez, 1970). However, the dehydration and rehydration (which involves disorder or structural collapse and subsequent restructuring) was not observed in this study, likely due to the specific characteristics of the sample, experimental conditions, interference from other substances or phases, etc. Although XRD analyses of cherts heated to 1000 °C are recorded after cooling to room temperature, the quartz inversion caused by decreasing temperature allowed the detection of low quartz.

The crystallinity of the *in situ* heat treated La Marañosa BE sample is much lower than that of the *in situ* heat treated Cerro Almodóvar B sample. In the *in situ* heat treated Cerro Almodóvar B sample the intensity decreasing of the main quartz and tridymite reflections from 25 ºC to 100 ºC coincides with the transformation observed in the 2D representation with false color of the *in situ* thermal difractogram pattern between 100-200 ºC, and would correspond to displacive transformations of low and high temperature form of tridymite (Richerson, 1992). The decreasing intensity of the main quartz and tridymite reflections between 500-600 ºC coincides with the transformation observed in the 2D representation with false color of the *in situ* thermal difractogram pattern between 500-600 ºC, and would correspond to the inversion of α-β quartz (Richerson, 1992). The transformation observed in the 2D representation with false color of the *in situ* thermal difractogram pattern between 800-900 ºC would correspond to reconstructive transformations of high quartz to tridymite (Fenner, 1913). On the other hand, up to 600 ºC a gradual change in the 2θ value of the reflection (101) occurred with *in situ* heating of the chert samples. Above this temperature, α-β quartz inversion temperature, the value of 2θ was maintained, at 800 ºC it decreased, coinciding with the high quartz to tridymite transformation, and increased again at higher temperatures.

The variations in FWHM of the reflections of quartz and cristobalite could suggest changes in the crystal quality or size with temperature. The (111) cristobalite reflection of the La Marañosa BE sample remaining fairly constant around 21.58 might suggest that the cristobalite structure is stable across the temperature range. The slight increase after cooling might indicate a minor structural change or relaxation after the thermal cycle. Higher FWHM values of cristobalite at lower temperatures indicate lower crystallinity or smaller

crystalline domains. The decrease in FWHM values of the cristobalite reflection (111) around 200-300°C might suggest an increase in crystallinity or growth of crystalline domains at these temperatures. The fluctuations at higher temperatures would indicate ongoing changes in the crystal structure or quality with temperature. Overall, these trends provide insights into the thermal stability and structural changes of quartz and cristobalite with temperature. In addition, if there is a change in the chert properties due to the heating treatment, that could be also have an effect their conservation (i.e., archaeological applications).

The progress of crystalline transformations in cherts, influenced by the dynamics of both *ex situ* and *in situ* heating, may alter the chert properties and influence e.g. the process of carving archaeological tools. Also, if there is a change in the chert properties due to the heating treatment, that could be also have an effect their conservation (i.e., archaeological applications). Heat treatment is a process used in archaeology to modify the properties of lithic raw materials to improve their knapping quality. This technique was practiced in southern Africa during the Middle Stone Age (Brown et al., 2009; Mourre et al., 2010; Porraz et al., 2013), it is known from the European Upper Palaeolithic, Mesolithic and Neolithic (Bordes, 1969; Binder, 1984; Tiffagom, 1998; Léa, 2005 and Eriksen, 2006), and the American Paleo-Indian period (Crabtree and Butler, 1964; Wilke et al., 1991).

6. Conclusions

The presence of moganite in the investigated cherts is independent of whether the chert is quartzitic or cristobalitic/tridymitic. *Ex situ* heat treated cherts cannot be differentiated into these types, as they may all contain quartz, cristobalite, and tridymite. In *ex situ* heat treated quartzitic cherts, some quartz transforms into tridymite and cristobalite high, and some monoclinic moganite transforms into orthorhombic moganite, coexisting with quartz low, tridymite, and/or cristobalite high. In *ex situ* heat treated cristobalitic/tridymitic cherts, the same siliceous phases are maintained, but cristobalite transforms into cristobalite high. Non-siliceous and silicate phases in the cherts transform into vitreous phases upon *ex situ* heating, some of which crystallize into new crystalline phases.

The temperatures of the quartz, tridymite, and cristobalite displacive and reconversion transformations observed in the cherts at 1000 ºC agree with those published in the literature. These conclusions highlight the importance of using both XRD and Raman spectroscopy for comprehensive chert analysis and understanding the complex thermal behavior of cherts. XRD and Raman spectroscopy are complementary techniques for detecting and quantifying moganite, with Raman spectroscopy capable of detecting lower concentrations and textural variations within the same sample. The 2D representation with false color of the *in situ* thermal diffractogram patterns is very useful for visualizing polymorphic transformations and dilation variations of the XRD reflections in the cherts. The analytical tools used to characterize the mineral phases of the investigated cherts provide a suitable and rapid alternative to conventional petrographic microscopy. Additionally, petrographic microscopy cannot effectively monitor the characteristics of cherts that have undergone alteration treatments, such as thermal or mechanical modifications.

The modification of the properties of cherts may vary depending on how the heat treatments are conducted. This is because the dynamics of *ex situ* and *in situ* heating of cherts affects the progress of crystalline transformations.

Finally, a correlation is observed between chert type (quartzitic and cristobalitic/tridymitic) and age, indicating a relationship between mineralogical composition and age. However, no correlation is found between elemental composition and age. Nevertheless, it is confirmed that the cherts examined in this study are biogenic. Still, further analysis of cherts is needed to confirm these observations.

Acknowledgements:

The authors wish to acknowledge the Scientific-Technical Services of the University of Oviedo (Spain) for X-ray diffraction. They would also like to thank the Barcelona Science Museum (Spain), Geominero Museum (Madrid, Spain) and Smithsonian Institution (Washington, USA) for providing chert samples for this research.

Funding:

This work was supported by Ministerio de Ciencia e Innovación (MCINN) project HAR2017-82557-P and MCIU-20-PCI2019-111931-2.

Competing interests

The authors declare none.

References

Adachi M., Yamamoto K., Sugisaki R. (1986) Hydrothermal chert and associated siliceous rocks from the northern Pacific their geological significance as indication of ocean ridge activity. *Sedimentary Geology*, **47**, 125-148. https://doi.org/10.1016/0037-0738(86)90075-8

Arthur M.A., Sageman B.B. (1994) Marine black shales: Depositional mechanisms and environments of ancient deposits. *Annual Review of Earth and Planetary Sciences*, **22**, 499-551. https://doi.org/10.1146/ANNUREV.EA.22.050194.002435

Binder D. (1984) Systèmes de débitage laminaire par pression: exemples chasséens provençaux. Pp 71-84 in: *Préhistoire de la pierre taillée, 2: économie du débitage laminaire: technologie et expérimentation: IIIe table ronde de technologie lithique* (J. Tixier, M.L. Inizan, H. Roche, editors) Meudon-Bellevue, Cercle de Recherches et d'Etudes Préhistoriques, Paris.

Boggs S. (2009) Petrology of sedimentary rocks (2nd ed., p 612). Cambridge, UK: Cambridge University Press.

Bordes F. (1969) Traitement thermique du silex au Solutréen. *Bulletin de la Société Préhistorique Française*, **66**, 197.

Brasier M., Green O., Shields G. (1997) Ediacarian sponge spicule clusters from southwestern Mongolia and the origins of the Cambrian fauna. *Geology*, **25**, 303-306. https://doi.org/10.1130/0091-7613(1997)025<0303:ESSCFS>2.3.CO;2

Brown K.S., Marean C.W., Herries A.I.R., Jacobs Z., Tribolo C., Braun D., Roberts D.L., Meyer M.C., Bernatchez J. (2009) Fire as an engineering tool of early modern humans. *Science* **325**, 859-862. DOI:10.1126/science.1175028

Bhuiya, A.K. and Stanley E. (1963) The refinement of atomic parameters by direct calculation of the minimum residual. Acta Cryst. **16**, 981-984

Chaklader A.C.D. (1961) Effect of trace Al_2O_3 on transformation of quartz to cristobalite. *Journal of the American Ceramic Society*, **44**(4), 175-180.

Chaklader A.C.D. (1963) X-Ray study of quartz-cristobalite transformation. *Journal of the American Ceramic Society*, **46**(2), 66-71.

Chaklader A.C.D., Roberts A.L. (1961) Transformation of quartz to cristobalite. *Journal of the American Ceramic Society*, **44**(1), 35-41.

Crabtree D.E., Butler B.R. (1964) Notes on experiment in flint knapping: 1. heat treatment of silica materials. *Tebiwa*, **7**, 1-6.

Dong Y., Xu S.L., Wen L., Chen H.D., Fu S.Y., Zhong Y.J., Wang J.Y., Zhu P., Cui Y (2020) Tectonic control of Guadalupian-Lopingian cherts in northwestern Sichuan Basin, South China. *Palaeogeography*, *Palaeoclimatology*, *Palaeoecology*, **557**, 109915. https://doi.org/10.1016/j.palaeo.2020.109915

Eriksen B.V. (2006) Colourful Lithics - the "Chaîne Opératoire" of Heat Treated Chert Artefacts in the Early Mesolithic of Southwest Germany. Pp 147-153 in: *After the Ice Age. Settlements, subsistence and social development in the Mesolithic of Central Europe* (C.J. Kind, editor). Konrad Theiss Verlag, Stuttgart.

Fenner C.N. (1913) The Stability Relations of the Silica Minerals. *American Journal of Sciences*, **36**, 331.

Fernández Alvarez T. (1970) Variación de|la superficie específica de la sepiolita precalentada a diferentes temperaturas. Bol. Soc. Esp. Cer., **9**(4), 377-394.

Flörke O.W., Flörke U., Giese U. (1984) Moganite: a new microcrystalline silica mineral. *Neues Jahrbuch für Mineralogie. Abhandlungen*, **149**, 325-336.

Gehling J.G., Rigby J.K. (1996) Long expected sponges from the Neoproterozoic Ediacara fauna of South Australia. *Journal of Paleontology*, **70**, 185-195. https://doi.org/10.1017/S0022336000023283

Götze J., Nasdala L., Kleeberg R. (1998) Occurrence and distribution of "moganite" in agate/chalcedony: A combined micro-Raman, Rietveld, and cathodoluminescence study. *Contributions to Mineralogy and Petrology*, **133**, 96-105. https://doi.org/10.1007/s004100050440

Graetsch H. and Flörke O. W. (1991) X-ray powder diffraction patterns and phase relationship of tridymite modifications. *Zeitschrift für Kristallographie*, **195**, 31-48

Heaney P.J. (1995) Moganite as an indicator for vanished evaporites: a testament reborn? *Journal of Sedimentary Research*, **65**A, 633-638. https://doi.org/10.1306/D4268180-2B26-11D7-8648000102C1865D

Heaney P.J., Post J.E. (2001) Evidence for an I2/a to Imab phase transition in the silica polymorph moganite at ~570 K. *American Mineralogist*, **86**, 1358-1366. https://doi.org/10.2138/am-2001-11-1204

Heaney P.J., Mckeown D.A., Post J.E. (2007) Anomalous behavior at the I2/a to Imab phase transition in SiO_2-moganite: An analysis using hard-mode Raman spectroscopy. *American Mineralogist*, **92**, 631-639. https://doi.org/10.2138/am.2007.2184

IGME (1972) . Mapa geológico de España. Hoja nº 419 (Villafranca del Penedés). Scale 1:50000).

IGME (1972). Mapa geológico de España. Hoja nº 953 (Lorca). Escala 1:50000

IGME (1973). Mapa geológico de España. Hoja nº 417 (Espluga de Francoli). Escala 1:50000

IGME (1973). Mapa geológico de España. Hoja nº 582 (Getafe). Escala 1:50000

IGME (1986). Mapa geológico de España. Hoja nº 559 (Madrid). Escala 1:50000

Kidder D.L., Erwin D.H. (2001) Secular distribution of biogenic silica through the Phanerozoic: Comparison of silica-replaced fossils and bedded cherts at the series level. *The Journal of Geology*, **109**, 509-522. https://doi.org/10.1086/320794

Kingma K.J., Hemley R.J. (1994) Raman spectroscopic study of microcrystalline silica. *American Mineralogist*, **79**, 269-273.

Kuellmer F.J., Poe T.I. (1964) The Quartz-Cristobalite Transformation. *Journal of the American Ceramic Society*, **47**(6), 311-312

Kuma R., Hasegawa H., Yamamoto K., Yoshida H., Whiteside J.H., Katsuta N., Ikeda M. (2019) Biogenically induced bedded chert formation in the alkaline palaeo-lake of the Green River formation. *Scientific Reports*, **9**, 16448. https://doi.org/10.1038/s41598-019-52862-7

Lampropoulou P., Xanthopoulou V., Wojtaszek-Kalaitzidi M., Petrounias P., Zoumpouli E., Iliopoulos G., Kalaitzidis S. (2022) Characterization of Siliceous Nodules in Western Kefalonia Island Greece: An Initial Approach to Their Formation and Diagenetic Characteristics. *Minerals*, **12**, 101. https://doi.org/10.3390/min12010101

Léa V. (2005) Raw, pre-heated or ready to use: discovering specialist supply systems for flint industries in mid-Neolithic (Chassey culture) communities in southern France. *Antiquity*, **79**, 1-15. https://doi.org/10.1017/S0003598X00113699

Mackenzie J.D. (1960) Fusion of Quartz and Cristobalite. *Journal of the American Ceramic Society*, **43**, 615-619. https://doi.org/10.1111/j.1151-2916.1960.tb13629.x

Maliva R.G., Knoll A.H., Simonson B.M. (2005) Secular change in the Precambrian silica cycle: Insights from chert petrology. *Geological Society of America Bulletin*, **117**, 835-845. https://doi.org/10.1130/B25555.1

Miehe G., Graetsch H. (1992) Crystal structure of moganite: A new structure type for silica. *European Journal of Mineralogy*, **4**, 693-706. https://doi.org/10.1127/ejm/4/4/0693

Mourre V., Villa P., Henshilwood C.S. (2010) Early use of pressure flaking on lithic artifacts at Blombos cave, South Africa. *Science*, **330**, 659-662. DOI: 10.1126/science.1195550

Müller, K.P. and Kolterman, M. (1965) Gasadsorption und Struktur von Sepiolith $Mg_8(H_2O)_4(OH)_4[Si_{12}O_{30}]\cdot n\ H_2O$. Z. Anorg. Alg. Chem., **341**, 36.

Murchey B.L., Jones D.L. (1992) A mid-Permian chert event: Widespread deposition of biogenic siliceous sediments in coastal, island arc and oceanic basins. *Palaeogeography, Palaeoclimatology, Palaeoecology*, **96**, 161-174. https://doi.org/10.1016/0031-0182(92)90066-E

Murray R.W. (1994) Chemical criteria to identify the depositional environment of chert: General principles and applications. *Sedimentary Geology*, **90**, 213-232. https://doi.org/10.1016/0037-0738(94)90039-6

Nukui A. and Flörke O. W. (1987) The tridymite structural modifications and cristobalite intergrown in one crystal. *American Mineralogist*, **72**, 167-169

Parthasarathy G., Kunwar A.C., Srinivasan R. (2001) Occurrence of moganite-rich chalcedony in Deccan flood basalts, Killari, Maharashtra, India. *European Journal of Mineralogy*, **13**, 127-134. https://doi.org/10.1127/0935-1221/01/0013-0127

Porraz G, Texier PJ, Archer W, Piboule M, Rigaud JP, Tribolo C (2013) Technological successions in the Middle Stone Age sequence of Diepkloof Rock Shelter, Western Cape, South Africa. *Journal of Archaeological Science*, **40**, 3376-3400. https://doi.org/10.1016/j.jas.2013.02.012

Preisinger, A. (1959) X-ray study of the structure of sepiolite: in Clays and Clay Minerals, 6th Conf., Pergamon Press, New York, pp. 61–67.

Richerson D.W. (1992) Modern ceramic engineering: Properties, processing and use in design, Marcel Dekker Inc., New York. https://doi.org/10.1201/9780429488245

Rodgers K.A., Cressey G. (2001) The occurrence, detection and significance of moganite (SiO_2) among some silica sinters. *Mineral Magazine*, **65**(2), 157-167. https://doi.org/10.1180/002646101550181

Roqué D.C. y Terradas X. (2016) Disponibilidad de rocas silíceas en el noreste peninsular: Resultados del proyecto LITOCATCPAG, 26, 245-282. ISSN: 2174-8063

Schneider H., Majdic A., Vasudevan R. (1986). Kinetics of the Quartz-Cristobalite Transformation in Refractory-Grade Silica Materials. Pp. 91-102 in: *Kinetics and Mass Transport in Silica and Oxide Systems*,**7**, (R. Freer and P.F Dennis, editors).

Shen B., Ma H.R., Ye H.Q., Lang X.G., Pei H.X., Zhou C.M., Zhang S.H., Yang R.Y. (2018) Hydrothermal origin of syndepositional chert bands and nodules in the Mesoproterozoic Wumishan Formation: Implications for the evolution of Mesoproterozoic cratonic basin, North China. *Precambrian Research*, **310**, 213-228. https://doi.org/10.1016/j.precamres.2018.03.007

Shoval S., Champagnon B., Panczer G. (1997) The quartz-cristobalite transformation in heated chert rock composed of micro and crypto-quartz by micro-raman and ftir spectroscopy methods. *Journal of Thermal Analysis*, **50**, 203-213. https://doi.org/10.1007/BF01979562

Shoval S., Erez Z., Kirsh Y., Deutsch Y., Kochavi M., Yadin E. (1989) Determination of the intensity of an early iron age conflagration at Tel-Hadar, Israel. *Thermochimica Acta*, **148**, 485-492. https://doi.org/10.1016/0040-6031(89)85251-7

Silvi B., D'Arco P., Saunders V.R., Dovesi R. (1991) Periodic Hartree-Fock study of minerals: tetracoordinated silica polymorphs. *Physics and Chemistry of Minerals*, **17**(8), 674-680

Sitarz M., Wyszomirski P., Handke B., Jelen P. (2014) Moganite in selected Polish chert samples: The evidence from MIR, Raman and X-ray studies. *Spectrochimica Acta, Part A: Molecular and Biomolecular Spectroscopy*, **122**, 55-58. https://doi.org/10.1016/j.saa.2013.11.039

Stevens S.J., Hand R.J., Sharp J.H. (1997) Polymorphism of silica. *Journal of Materials Science*, **32**, 2929-2935. https://doi.org/10.1023/A:1018636920023

Stoch L., Łaczka M., Wacławska I. (1985) DTA and x-ray diffraction study of the phase transformation of silica minerals. *Thermochimica Acta*, **93**, 533-536

Tatzel M., von Blanckenburg F., Oelze M., Schuessler J.A., Bohrmann G. (2015) The silicon isotope record of early silica diagenesis. *Earth and Planetary Science Letters*, **428**, 293-303. https://doi.org/10.1016/j.epsl.2015.07.018

Thompson A.B. and Wennemer M. (1979) Heat capacities and inversions in tridymite, cristobalite, and tridymite-cristobalite mixed phases. *American Mineralogist*, **64**(9-10), 1018-1026

Tucker M. E. (2001) Sedimentary petrology. London, UK: Blackwell, Scientific Publication.

Turekian K.K. and Wedepohl K.H. (1961) Distribution of the elements in sorne major units of the earth's crust. *The Geological Society of America Bulletin*, **72**, 175-192

Tiffagom M. (1998) Témoignages d'un traitement thermique des feuilles de laurier dans le Solutréen supérieur de la grotte du Parpalló (Gandia, Espagne). *Paleo*, **10**, 147-161.

USGS (2006). Mapa geológico de Venezuela. Hoja 1. Escala 1:750.000

Uribe-Zorita de M., Álvarez-Lloret P., Bottura S., Marcos C. (2023) Characterization of Color and Composition in Chert for Grouping and Comparison. *Global Journal of Archaeology and Anthropology*, **13**, 1-5. https://doi.org/10.19080/gjaa.2023.13.555858

Westacott S., Planavsky N.J. Zhao, M.-Y., Hull P.M. (2021) Revisiting the sedimentary record of the rise of diatoms. *Proceedings of the National Academy of Sciences of the United States of America*, **118**. https://doi.org/10.1073/PNAS.2103517118

Whitney DL, Evans BW (2010) Abbreviations for names of rock-forming minerals. *American Mineralogist*, **95**, 185-187. DOI: 10.2138/am.2010.3371

Wilke P.J., Flenniken J., Ozbun T.L. (1991) Clovis Technology at the Anzick Site, Montana. *Journal of California and Great Basin Anthropology*, **13**, 242-272.